

Common Design Principles in the Spliceosomal RNA Helicase Brr2 and in the Hel308 DNA Helicase

Vladimir Pena,^{1,2,7} Sina Mozaffari Jovin,^{1,7} Patrizia Fabrizio,¹ Jerzy Orłowski,^{3,4} Janusz M. Bujnicki,^{3,5} Reinhard Lührmann,^{1,*} and Markus C. Wahl^{2,6,*}

¹Abteilung Zelluläre Biochemie

²AG Röntgenkristallographie

Max-Planck-Institut für Biophysikalische Chemie, Am Faßberg 11, D-37077 Göttingen, Germany

³Laboratory of Bioinformatics and Protein Engineering, International Institute of Molecular and Cell Biology, Ul. Ks. Trojdena 4, PL-02-109 Warsaw, Poland

⁴PhD School at the Institute of Biochemistry and Biophysics PAS, Ul. Pawinskiego 5a, PL-02-106 Warsaw, Poland

⁵Bioinformatics Laboratory, Institute of Molecular Biology and Biotechnology, Adam Mickiewicz University, Ul. Umultowska 89, PL-61-614 Poznan, Poland

⁶Freie Universität Berlin, Fachbereich Biologie, Chemie, Pharmazie, Institut für Chemie und Biochemie, AG Strukturbiochemie, Takustraße 6, D-14195 Berlin, Germany

⁷These authors contributed equally to this work

*Correspondence: reinhard.luehrmann@mpi-bpc.mpg.de (R.L.), mwahl@gwdg.de (M.C.W.)

DOI 10.1016/j.molcel.2009.08.006

SUMMARY

Brr2 is a unique DExD/H box protein required for catalytic activation and disassembly of the spliceosome. It contains two tandem helicase cassettes that both comprise dual RecA-like domains and a noncanonical Sec63 unit. The latter may bestow the enzyme with unique properties. We have determined crystal structures of the C-terminal Sec63 unit of yeast Brr2, revealing three domains, two of which resemble functional modules of a DNA helicase, Hel308, despite lacking significant sequence similarity. This structural similarity together with sequence conservation between the enzymes throughout the RecA-like domains and a winged helix domain allowed us to devise a structural model of the N-terminal active cassette of Brr2. We consolidated the model by rational mutagenesis combined with splicing and U4/U6 di-snRNA unwinding assays, highlighting how the RecA-like domains and the Sec63 unit form a functional entity that appears suitable for unidirectional and processive RNA duplex unwinding during spliceosome activation and disassembly.

INTRODUCTION

Most eukaryotic precursor messenger RNAs (pre-mRNAs) contain noncoding intervening sequences. These introns have to be removed and the coding sequences (exons) have to be ligated during pre-mRNA splicing to produce mature mRNA for protein biosynthesis. Pre-mRNA splicing involves two sequential transesterification steps that are facilitated by a large and dynamic ribonucleoprotein (RNP) enzyme, the spliceosome (reviewed in Wahl et al. [2009]). Active spliceosomes form only in the presence of a pre-mRNA substrate, on which they are

assembled stepwise from small nuclear ribonucleoprotein particles (snRNPs; U1, U2, U4/U6, and U5) and numerous non-snRNP splicing factors (reviewed in Brow, [2002]).

Spliceosome assembly is initiated by U1 snRNP binding to the 5' splice site (SS) followed by U2 snRNP recognizing a conserved branch point sequence in the intron. Subsequently, the other snRNPs join as a preformed U4/U6-U5 tri-snRNP, giving rise to a precatalytic spliceosome that is still inactive. This particle has to undergo massive compositional and conformational rearrangements to become catalytically competent for the first step. Further remodeling generates a spliceosome that catalyzes the second step. Finally, the postcatalytic complex is disassembled in an ordered fashion.

The above scenario involves profound changes in the spliceosomal RNA network and the dynamic exchange of many proteins (reviewed in Wahl et al. [2009]). For example, in the U4/U6-U5 tri-snRNP, the U4 and U6 RNAs form two intermolecular double helices (stem I and stem II) that in yeast comprise 8 and 17 base pairs, respectively, representing the most stable RNA duplex of the spliceosome (Brow and Guthrie, 1988). This interaction has to be broken during catalytic activation so that U6 RNA can rearrange to form catalytically important structures and engage in alternative interactions with the 5' SS and with U2 RNA. U4 RNA and all U4/U6-specific proteins are removed in the process.

The RNP-remodeling events during pre-mRNA splicing are driven by more than ten DExD/H box ATPases/RNA helicases (reviewed in Staley and Guthrie [1998] and Wahl et al. [2009]). Most of these enzymes associate transiently with the spliceosome and are thought to act in a nonprocessive manner by locally destabilizing short RNA duplexes or by remodeling a confined RNA-protein network. Their modes of action may resemble that of DEAD box proteins, which load onto and locally destabilize double helices without translocating on the substrate nucleic acid (Yang et al., 2007).

DEAD box proteins are unsuitable for efficient unwinding of long duplexes with two or more helical turns (Yang et al., 2007), suggesting that unwinding of U4 and U6 during spliceosome

catalytic activation requires a distinct mechanism. Indeed, unwinding of the U4/U6 duplex depends on the Brr2 (U5-200K) protein (Laggerbauer et al., 1998; Raghunathan and Guthrie, 1998), which functionally differs from all other spliceosomal RNA helicases. Brr2 is an integral component of the U5 snRNP (Lauber et al., 1996; Noble and Guthrie, 1996) and enters the spliceosome as part of the U4/U6-U5 tri-snRNP before catalytic activation; thereafter, it remains stably associated with the catalytic core of the spliceosome (Bessonov et al., 2008). In addition to catalytic activation, Brr2 is again required during spliceosome disassembly (Small et al., 2006). It is the only spliceosomal helicase that belongs to the Ski2-like subfamily of the superfamily 2 (SF2) helicases (Bleichert and Baserga, 2007). The protein is one of the largest spliceosomal factors (246 kDa in yeast). It contains an N-terminal region (residues 1–495 of yeast Brr2) predicted to lack stable tertiary structure and a tandem repeat of helicase cassettes (residues 496–1310 and 1311–2163 for N- and C-terminal cassettes, respectively). Both cassettes comprise dual RecA-like domains followed by a region that bears resemblance to a portion of the Sec63p subunit of the protein translocation apparatus of the endoplasmic reticulum (herein referred to as Sec63 units) (Ponting, 2000). Although RecA-like domains are common to all helicases, only Brr2, the Ski2-like helicase 1 (Slh1, a putative RNA helicase implicated in antiviral defense bearing a similar tandem cassette arrangement as Brr2) (Martegani et al., 1997), and the Mer3/HFM1 family of DNA helicases (Ponting, 2000) are predicted to contain Sec63 units. The conserved domain structure and sequence (Figure S1 available online) suggest that the two cassettes of Brr2 originated from a gene duplication event and subsequently diverged. Only the N-terminal cassette of Brr2 is essential for U4/U6 RNA unwinding, whereas the C-terminal cassette tolerates catalytically detrimental mutations in active site motifs (Kim and Rossi, 1999) and may have evolved into a protein-protein interaction platform (Liu et al., 2006; van Nues and Beggs, 2001).

Here, we investigated whether the noncanonical Sec63 units confer special mechanistic features on Brr2 (all proteins used in this work were from yeast). We determined crystal structures of the C-terminal Sec63 unit of Brr2, revealing a close structural similarity to helicase-associated domains of the archaeal Hel308 DNA helicase (Buttner et al., 2007). Taking advantage of sequence conservation throughout the remainder of the helicases and between the C- and N-terminal cassettes of Brr2, we devised a structural model of the N-terminal functional cassette of Brr2 and tested aspects of the model by mutational analysis. We suggest that, analogous to the organization of Hel308, the Sec63 unit of the N-terminal helicase cassette of Brr2 is an integral component of the active site, which is functionally connected to the RecA-like domains by a winged helix (WH) module. This architecture may allow Brr2 to processively unwind the extended U4/U6 duplex during spliceosome catalytic activation.

RESULTS AND DISCUSSION

Structural Organization of a Sec63 Unit

Guided by domain annotation (Ponting, 2000), secondary structure prediction, and fold recognition, we cloned portions of Brr2

comprising the N- or the C-terminal Sec63 units. Among more than ten expression constructs, only the region spanning residues 1839–2163, which contained the predicted C-terminal Sec63 unit (Sec63^C), could be expressed as a soluble protein in *Escherichia coli*. Purified Brr2^{1839–2163} eluted according to its monomeric molecular weight in analytical size exclusion chromatography and reproducibly yielded two well-diffracting crystal forms (Table 1), indicating that it encompasses an autonomously folded unit. The form 1 structure was solved by the single anomalous dispersion (SAD) strategy after soaking of a crystal with bromide and was refined against 1.65 Å resolution data from a native crystal (Table 1 and Figure 1A). The structure of the second form was solved by molecular replacement and refined at 2.0 Å resolution (Table 1 and Figure 1B). The entire residue range, 1839–2163, could be traced in the first crystal structure, whereas a short N-terminal peptide (residues 1839–1843) was disordered in the second structure. The final models exhibited low R_{work} and R_{free} factors with good stereochemistry (Table 1).

Sec63^C comprises three domains that are arranged in a triangle with maximum orthogonal dimensions of 74.4 Å, 61.1 Å, and 54.8 Å (Figures 1A and 1B). An oval-shaped N-terminal domain (domain 1, residues 1859–1990; blue in Figures 1A and 1B) encompasses six α helices (α 1– α 6) and one 3_{10} helix (3_{10} 1). Its long dimension is defined by helix α 5, which acts as a scaffold for the other five helices, which associate via hydrophobic contacts to form a six-helix bundle. The central domain (domain 2, residues 1991–2048; red in Figures 1A and 1B) adopts a helix-loop-helix (HLH) fold, comprising helices α 7– α 10 and a second 3_{10} helix (3_{10} 2). The C-terminal domain (domain 3, residues 2049–2163; green in Figures 1A and 1B) adopts a seven-stranded immunoglobulin-like β sandwich, in which the outer sheet is composed of strands β 1, β 2, and β 5 and the inner sheet is composed of strands β 3, β 4, β 6, and β 7. The N-terminal 20 residues (1839–1858) constitute a flexible tail that lacks regular structure and is differently oriented in the two crystal forms (black in Figures 1A and 1B). Excluding the N-terminal tails, the two structures are very similar, exhibiting a root-mean-square deviation (rmsd) of 0.53 Å for 307 C α positions. While this paper was under review, a very similar structure of a Sec63 unit comprising residues 1851–2163 of yeast Brr2 was published (rmsd 0.52 Å and 0.59 Å for 307 and 309 C α positions compared to our structures; Zhang et al., 2009).

Each domain of Sec63^C is in contact with the other two, and the domain arrangement is independent of the two different crystal environments (Figures 1A and 1B). 446 Å² of combined surface area are buried in the contact of domains 1 and 2; 2060 Å² are buried between domains 1 and 3; and 1078 Å² are buried between domains 2 and 3. The β sandwich domain 3 can be regarded as the integrating element of the domain assembly. Large loops connecting strands β 2 and β 3 (23 residues) and strands β 6 and β 7 (7 residues) of domain 3 protrude toward the center of the Sec63^C structure and seem to fix the domains relative to each other (Figure 1C). Although they lack regular secondary structure, these contact loops exhibit identical conformations in the two different crystal forms.

Table 1. Crystallographic Data

Data Collection	Native 1	Native 2	Br Peak	Br Infl.	Br HE ^a Rem.
Wavelength (Å)	1.050	1.050	0.9120	0.9120	0.90
Temperature (K)	100	100	100	100	100
Space group	P2 ₁ 2 ₁ 2 ₁	P4 ₁ 2 ₁ 2	P2 ₁ 2 ₁ 2 ₁	P2 ₁ 2 ₁ 2 ₁	P2 ₁ 2 ₁ 2 ₁
Unit cell parameters					
a	55.2	104.1	55.1	55.1	55.1
b	76.5	104.1	76.2	76.2	76.2
c	84.6	77.4	84.5	84.5	84.5
Resolution (Å)	30.0 – 1.65 (1.70 – 1.65) ^b	30.0 – 2.0 (2.12 – 2.00)	30.0 – 2.0 (2.10 – 2.00)	30.0 – 2.0 (2.11 – 2.00)	30.0 – 2.0 (2.13 – 2.00)
Reflections					
Unique	43474 (3448)	29516 (4612)	44408 (4752) ^c	44549 (4973)	47581 (5834)
Completeness (%)	99.0 (99.7)	99.2 (99.3)	98.3 (87.3)	98.8 (91.5)	99.8 (100)
Redundancy	4.3 (4.2)	3.1 (3.2)	7.6 (6.8)	3.8 (3.7)	3.8 (3.7)
I/σ(I)	30.5 (2.1)	13.7 (1.7)	29.1 (3.5)	17.9 (1.4)	17.2 (1.9)
R _{sym} (I) ^d	0.06 (0.51)	0.10 (0.56)	0.07 (0.54)	0.05 (0.75)	0.05 (0.70)
Phasing					
Resolution (Å)	Br Sites	SHELX CC/CC _{weak} ^e	SHELXE CC _{overall}	CC _{free} Left/Right Hand	FOM ^f
30.0–2.0	28	32.4/15.7	24.6	50.8/27.5	0.49
Refinement					
Native 1		Native 2			
Resolution (Å)	20.0 – 1.65 (1.69 – 1.65)		20.0 – 2.0 (2.04 – 2.00)		
Reflections					
Number	43382 (3156)		29478 (2022)		
Completeness (%)	99.0 (99.6)		99.0 (93.9)		
Test set (%)	5.0		5.1		
Refined residues/atoms					
Protein	325/2726		320/2697		
Water	412		352		
R _{work} ^g	19.3 (34.5)		18.8 (25.9)		
R _{free} ^g	23.2 (37.5)		23.7 (30.4)		
ESU (Å) ^h	0.075		0.106		
Mean B factors (Å ²)					
Wilson	32.0		35.3		
Protein	32.5		35.9		
Water	48.0		46.5		
Ramachandran plot ⁱ					
Favored	98.45		99.06		
Outliers	0		0		
Rmsd geometry					
Bond lengths (Å)	0.013		0.012		
Bond angles (°)	1.24		1.19		
Rmsd B factors (Å ²)					
Main chain bonds	0.55		0.38		
Main chain angles	0.93		0.62		
Side chain bonds	1.54		0.97		
Side chain angles	2.36		1.54		
PDB ID	3IM1		3IM2		

^a HE, high energy.^b Data for the highest-resolution shell in parentheses.^c Numbers of unique reflections are given after averaging of Friedel pairs for the native data sets and with Friedel pairs kept separate for Br data sets with anomalous signals.

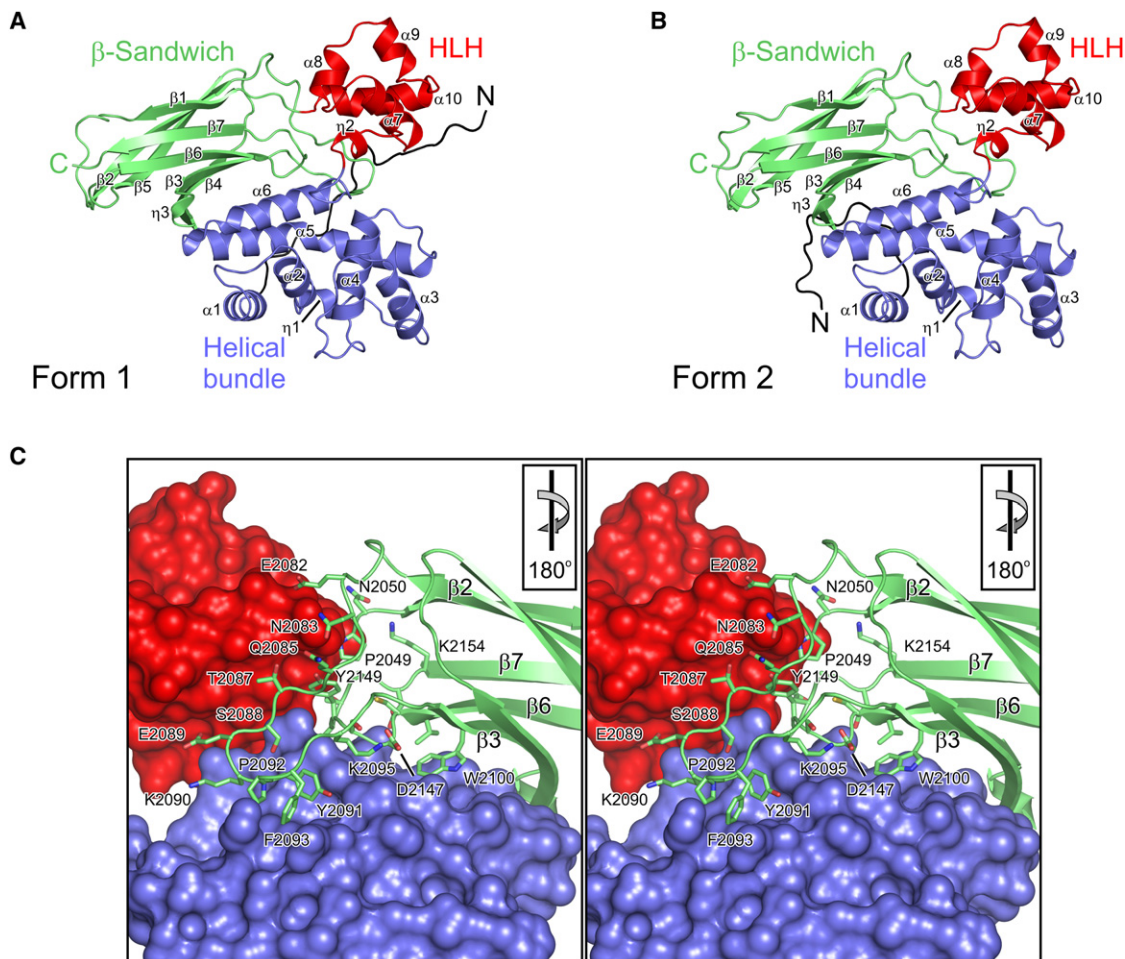


Figure 1. Structural Overview of the C-Terminal Sec63 Unit of Brr2

(A and B) Ribbon plots of two forms of Sec63^C from Brr2. Secondary structure elements are labeled. Steel blue, helical bundle domain; red, HLH domain; green, β sandwich domain. N-terminal tails, which lack regular structure and adopt different orientations in the two crystal forms, are shown in black. (C) Stereo plot of the domain interactions. The $\beta 2$ - $\beta 3$ and $\beta 6$ - $\beta 7$ loops of the β sandwich domain (green) intimately interact with the helical bundle domain (steel blue) and the HLH domain (red). Interface residues are labeled. The view is 180° compared to the view in (A) and (B) as indicated.

The Sec63^C Unit Provides a Suitable Model for the Sec63^N Unit of the Catalytic Cassette of Brr2

The overall sequences of the N- and C-terminal Sec63 units of Brr2 are 20% identical, suggesting that they contain the same structural modules (Ponting, 2000). However, a significantly larger proportion of the residues lining the domain interfaces of Sec63^C are retained in Sec63^N (40% identity) (Figure S1). The extensive hydrophobic and van der Waals interdomain interactions in Sec63^C involve conserved residues of the helical

bundle domain (V1962, M1977, and V1987), the HLH domain (R1995, Q1996, and Y2048), and the β sandwich domain (Y2149, L2150, W2100, V2102, and L2111). In addition, conserved polar contacts occur between the helical bundle domain and the β sandwich domain (N1959-D2147 and Q1981-D2153). Significantly, these interface residues are also conserved between species (Figure S1). These observations suggest that the present structures of Sec63^C provide suitable models for the Sec63^N unit associated with the catalytically

^d $R_{\text{sym}}(I) = \sum_{hkl} \sum_i |I_i(hkl) - \langle I(hkl) \rangle| / \sum_{hkl} \sum_i |I_i(hkl)|$; for n independent reflections and i observations of a given reflection; $\langle I(hkl) \rangle$, average intensity of the i observations.

^e $CC = [\sum w E_o E_c \sum w - \sum w E_o \sum w E_c] / \{[\sum w E_o^2 \sum w - (\sum w E_o)^2] [\sum w E_c^2 \sum w - (\sum w E_c)^2]\}^{1/2}$; w , weight (see http://shelx.uni-ac.gwdg.de/SHELX/shelx_de.pdf for full definitions).

^f FOM, figure of merit = $|F(hkl)_{\text{best}}| / |F(hkl)|$; $F(hkl)_{\text{best}} = \sum_{\alpha} P(\alpha) F_{hkl}(\alpha) / \sum_{\alpha} P(\alpha)$.

^g $R = \sum_{hkl} |F_{\text{obs}} - F_{\text{calc}}| / \sum_{hkl} F_{\text{obs}}$; $R_{\text{work}} - hkl \notin T$; $R_{\text{free}} - hkl \in T$; T , test set.

^h ESU, estimated standard uncertainties (estimated overall coordinate error) based on maximum likelihood.

ⁱ Calculated with MolProbity (<http://molprobity.biochem.duke.edu/>) (Davis et al., 2004).

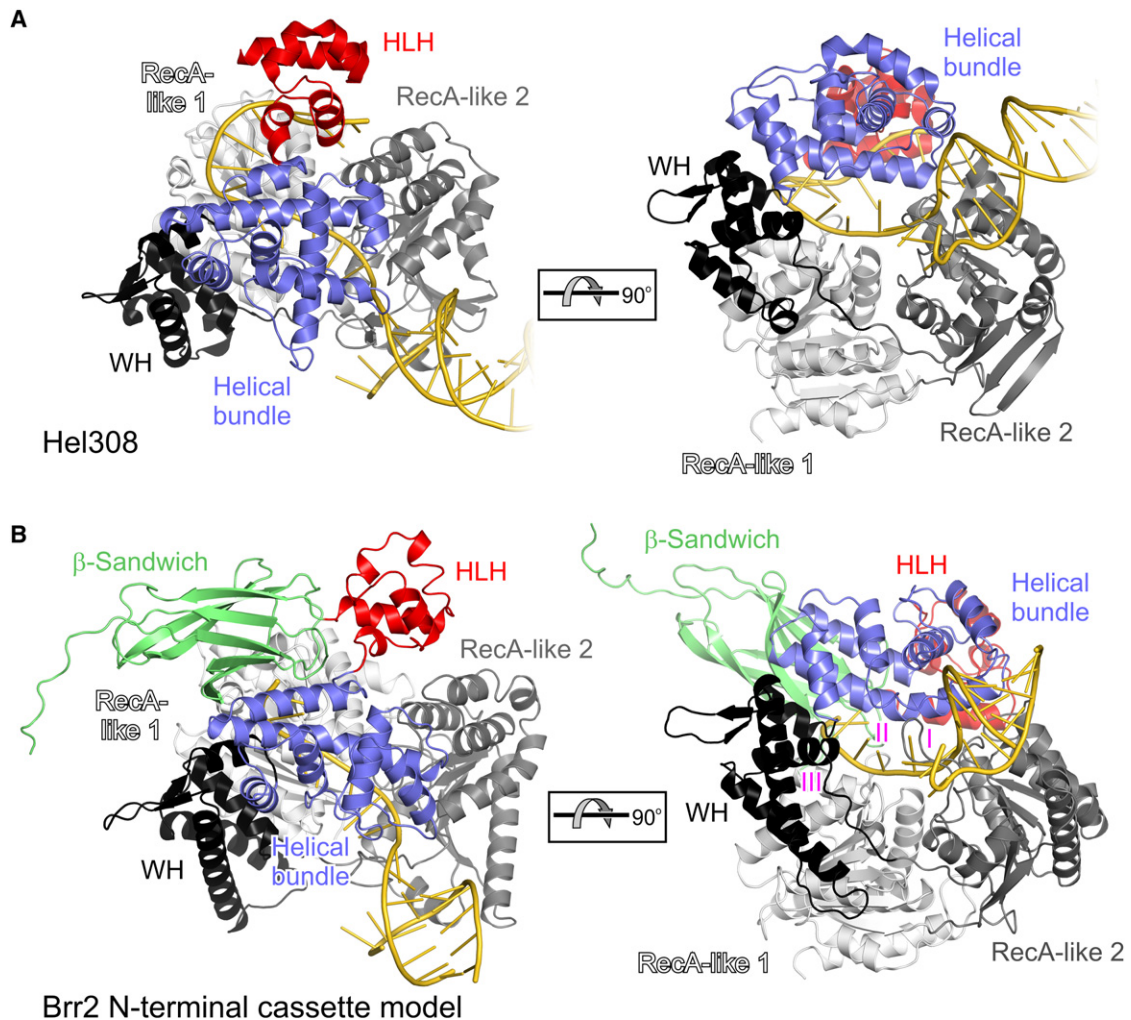


Figure 2. Model of the Catalytic N-Terminal Cassette of Brr2

(A) Orthogonal ribbon plots of the Hel308 DNA helicase (Buttner et al., 2007) (PDB ID 2P6R). Light and dark gray, RecA-like domains; black, WH domain; steel blue, helical bundle domain; red, HLH domain; gold, DNA. In the left panel, the helical bundle domain is oriented as in Figures 1A and 1B.

(B) Orthogonal ribbon plots of the model of the N-terminal cassette of Brr2. Green, β sandwich domain; gold, RNA; other domains are colored as before. Regions in I, II, and III were investigated by mutational analysis. I, putative separator loop in the second RecA-like domain; II, underside of helix $\alpha 5$ of the helical bundle domain; III, WH domain interfaces. In the left panel, the Sec63 unit is oriented as in Figures 1A and 1B.

active N-terminal cassette of Brr2. Consistent with this conclusion, when we used bioinformatics methods, protein fold recognition, and comparative modeling to obtain a structural model of the N-terminal Sec63 unit of Brr2, the internal architecture of the Sec63^N model closely resembled the experimental Sec63^C structure. Modeling also indicated the same global fold for the Sec63 units from Slh1, Mer3/HFM1, and the translocon Sec63p. In contrast to the conserved fold, the surfaces of the Sec63 units have apparently diverged (Figure S2; illustrated for example by differences in the electrostatic surface potentials between the structure of Sec63^C and the model of Sec63^N), consistent with the idea that the C-terminal cassette of Brr2 has selectively evolved into a hot spot of protein-protein interactions in the spliceosome (Liu et al., 2006; van Nues and Beggs, 2001).

Two Domains of Sec63^C Resemble Modules of the Hel308 DNA Helicase

The above results provide a structural model for the Sec63^N unit but do not reveal how it may contribute to Brr2 function. However, comparison of our Sec63^C structures with Protein Data Bank entries revealed that the helical bundle domain 1 and the HLH domain 2 closely resemble two structural modules of Hel308, a processive 3'-to-5' DNA helicase involved in DNA repair at replication forks (Buttner et al., 2007; PDB ID 2P6R; Figure 2A), despite low overall sequence identity (16% throughout both domains). The helical bundle domain 1 of Sec63^C and domain 4 of Hel308 can be aligned with an rmsd of 3.1 Å for 124 C α atoms; the HLH domain of Sec63^C aligns with an rmsd of 2.5 Å over 49 residues with the HLH domain (domain 5) of Hel308. The relative orientations of the domains 1 and 2 in Sec63^C and of the

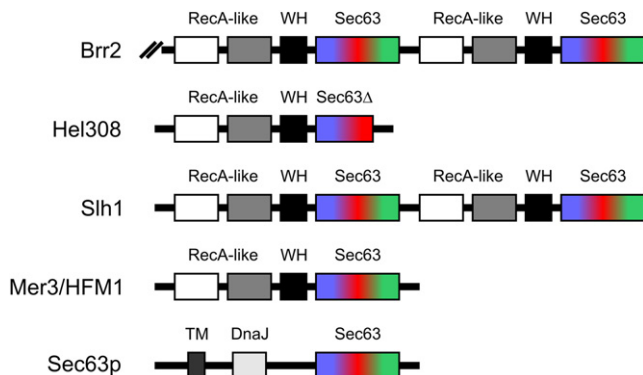


Figure 3. Proteins Harboring Sec63 Units

Schematic representation of the domain organization of proteins bearing Sec63 units. WH, winged helix domain; Sec63 Δ , truncated Sec63 unit of Hel308; TM, transmembrane domain of the translocon Sec63p; DnaJ, DnaJ domain.

corresponding domains 4 and 5 in Hel308 differ slightly, perhaps because Hel308 lacks an equivalent of the β sandwich domain that secures the relative orientation of the other two domains in Sec63^C. Thus, structural comparison shows that Hel308 bears a truncated Sec63 unit that encompasses only a helical-bundle domain and an HLH domain (Figure 3), previously disguised by the disparate sequences of Hel308 and the Brr2 Sec63 units throughout this region (Figure S1). We therefore went on to explore whether Hel308 and Brr2 share additional design principles and perhaps mechanistic aspects.

A WH Domain Precedes the Sec63 Unit in Both Cassettes of Brr2

The truncated Sec63 unit of Hel308 is preceded by a WH domain that connects it to the catalytic RecA-like domains (Figures 2A and 3). Our crystallized Brr2 fragment contained an N-terminal stretch (residues 1840–1858), which does not form an integral part of the Sec63^C unit although it is highly conserved among Brr2 orthologs (Figure S1 and black in Figures 1A and 1B). The Sec63p subunit of the protein translocation machinery lacks a corresponding N-terminal expansion (Figure S1), showing that a canonical Sec63 unit is shorter than originally predicted (Ponting, 2000). Instead, the N-terminal appendix of our structure exhibits high sequence similarity to the C-terminal part of the WH domain of Hel308 (>50% identity) (Figure S1). Multiple sequence alignments revealed that not only the N-terminal appendix, but rather the entire WH domain and the two RecA-like domains of Hel308 are conserved in both cassettes of Brr2 (Figure S1). Thus, the Brr2 fragment that we have expressed bears only part of a WH domain, explaining why this portion is structurally unstable (Figures 1A and 1B). We subsequently attempted but failed to express Brr2 fragments encompassing a full WH domain in soluble form. Taken together, our findings suggest that both cassettes of Brr2 structurally closely resemble each other, although they may serve different functions, and that, in both cassettes, dual RecA-like domains are connected via a WH domain to a Sec63 unit, matching the organization of the related Hel308 DNA helicase.

A Structural Model of the N-Terminal Catalytic Cassette of Brr2

Our crystal structure of the Sec63^C unit, the similarity between N- and C-terminal cassettes of Brr2, and the similarity of both of these cassettes to Hel308 provided us with the tools to devise structural models of the C-terminal inactive cassette as well as of the N-terminal catalytic cassette of Brr2. We used the crystal structures of the Hel308 helicase and of Sec63^C as templates for modeling of both cassettes, employing the GeneSilico Meta-Server (Kurowski and Bujnicki, 2003) to generate target-template alignments and the FRANKENSTEIN'S MONSTER approach (Kosinski et al., 2005) to build an optimized three-dimensional atomic representation. In the resulting models of both cassettes, all domains pack without clashes, including the β sandwich domain that is not contained in Hel308 (Figure 2B). In the models, the amino acids populate the secondary structure elements largely as expected from their predicted secondary structure propensities. Furthermore, the model quality assessment method MetaMQAP (Pawlowski et al., 2008) predicted that the theoretical models exhibit 2.7 and 2.6 C α rmsd with respect to the true (currently unknown) structures of the N- and C-terminal cassettes, respectively, suggesting that they might be useful as medium-resolution working models of the protein structure.

In Hel308, the two RecA-like domains (light and dark gray in Figure 2A), the WH domain (black in Figure 2A), and the helical bundle domain of the truncated Sec63 unit (blue in Figure 2A) form a circular arrangement with a central tunnel, through which one strand of the DNA substrate is threaded. The two Brr2 cassettes can be modeled into a similar circular domain arrangement bearing a central tunnel backed by the HLH and the β sandwich domain (Figure 2B). In order to explore whether the N-terminal cassette of Brr2 may bind RNA in a similar fashion as DNA is bound by Hel308, we calculated the electrostatic surface potential of the corresponding model. Strikingly, the interior and one flank of the predicted central tunnel of the N-terminal cassette exhibit a strongly positive surface potential, suitable for the interaction with the negatively charged sugar-phosphate backbone of RNA (Figure S3). In contrast, in the model of the C-terminal cassette, the corresponding regions are lined with more electro-negative and mixed surface potentials (Figure S3), corroborating the idea that it does not serve for RNA binding and unwinding. We also modeled the helicase cassettes of Slh1 and Mer3/HFM1 (Figure S3). Mer3/HFM1 and the N-terminal cassette of Slh1 exhibit a similar surface potential to the N-terminal cassette of Brr2, and these proteins are known or expected to be active helicases. The C-terminal cassette of Slh1, as in Brr2, lacks the positive surface around the tunnel and thus may be inactive.

If Brr2 followed the nucleic-acid-binding mechanism of Hel308, it should contact single-stranded 3' overhangs. Consistently, many Hel308 residues that contact the DNA single-stranded overhang are conserved in Brr2 (Figure S1), and these Brr2 residues project into the inner tunnel of the modeled N-terminal cassette (Figure S4). We also tested this prediction by electrophoretic mobility shift assays using recombinant Brr2 expressed in yeast and the yeast U4/U6 RNA as a putative substrate. In this and all of the following experiments, we employed gel-purified RNA duplexes and highly pure recombinant Brr2 (Figure S5). As expected, Brr2 efficiently bound wild-type

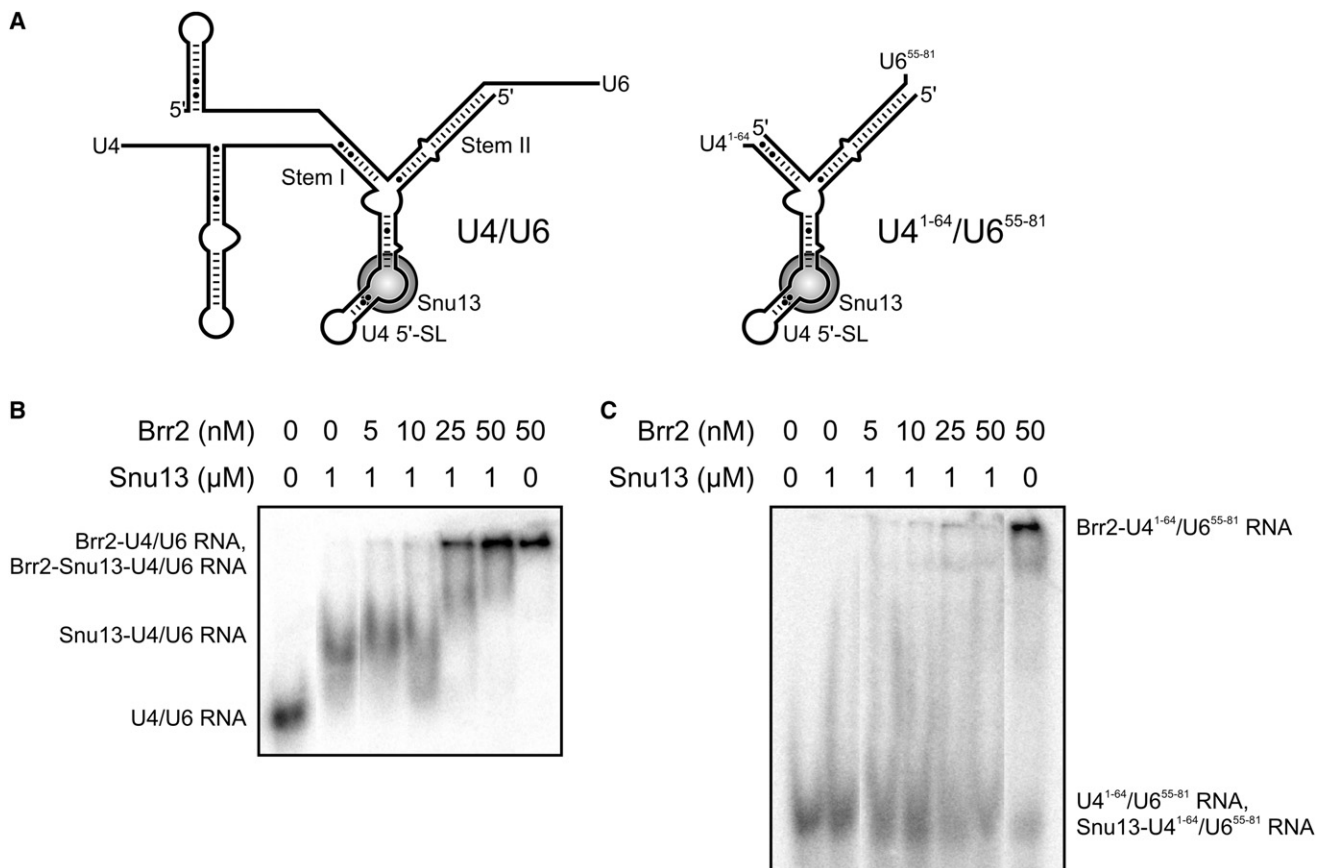


Figure 4. RNA Binding by Brr2

(A) RNA duplexes employed. Landmark elements of the duplexes (stem I, stem II, and U4 5' SL) and Snu13 binding are indicated.

(B) Gel shift (6% gel) monitoring the binding of Brr2 (increasing concentrations as indicated) to full-length U4/U6 RNA (0.5 nM; U6 labeled) in the presence and absence of 1 μM Snu13. RNA was incubated with Snu13 for 20 min at 4°C and additionally for 15 min at 30°C after addition of Brr2. All lanes are from the same gel. Brr2 complexes have migrated into the gel, as more clearly seen in Figure S7.

(C) Gel shift (6% gel) monitoring the binding of Brr2 (increasing concentrations as indicated) to U4¹⁻⁶⁴/U6⁵⁵⁻⁸¹ RNA (0.5 nM; U4¹⁻⁶⁴ labeled) in the presence and absence of 1 μM Snu13. Samples were prepared as in (B). All lanes are from the same gel. At the present gel concentration, the Snu13-U4¹⁻⁶⁴/U6⁵⁵⁻⁸¹ RNA complex was not resolved from the U4¹⁻⁶⁴/U6⁵⁵⁻⁸¹ RNA alone.

(WT) U4/U6 RNA but exhibited much reduced affinity for a truncated U4¹⁻⁶⁴/U6⁵⁵⁻⁸¹ RNA, lacking single-stranded overhangs except for a single G residue at the 5' end of U4¹⁻⁶⁴ and at the 3' end of U6⁵⁵⁻⁸¹ (Figure 4). Binding of Brr2 to U4¹⁻⁶⁴/U6⁵⁵⁻⁸¹ RNA was completely abolished in the presence of Snu13, which binds the U4 5' stem loop (SL) (Liu et al., 2007; Vidovic et al., 2000), whereas binding to full-length U4/U6 RNA was unaffected by Snu13 (Figure 4). Binding of Snu13 sequesters single-stranded regions of the U4 5' SL in the form of a K turn, which may otherwise provide a fortuitous binding site for Brr2. Snu13 may also discourage Brr2 binding to the truncated duplex by reducing breathing of stems I and II, which neighbor its binding site (Figure 4).

Mutational Analysis Supports the Architectural Model of Brr2

Upon closer inspection, our structural model predicts a number of mechanistic features associated with the catalytic N-terminal cassette of Brr2. Thus, in order to further validate the model, we

probed the N-terminal cassette of Brr2 by targeted mutational analysis in vivo.

A Putative Strand Separation Device in the Second RecA-like Domain

In the cocrystal structure of Hel308, a β hairpin between helicase motifs V and VI (Tanner and Linder, 2001) of the second RecA-like domain is inserted between the two strands of the DNA substrate (Buttner et al., 2007) (Figure 5A, left). Aromatic residues in this element stack with the nucleic acid bases and seem to act as a strand separation device, although the function of this element has not been addressed experimentally. Mutations in an equivalent of this β hairpin in the processive hepatitis C virus NS3 RNA helicase abolish duplex unwinding without affecting ATPase activity (Lam et al., 2003). The β hairpin is also predicted in other Ski2-like helicases, including Slh1, Mer3/HFM1, and Brr2 (Figure S1). All predicted loops contain aromatic residues whose exact positions differ slightly. In our model of Brr2, the predicted loop contains a tyrosine (Y853) and a tryptophan (W860) and is wedged between the nucleic

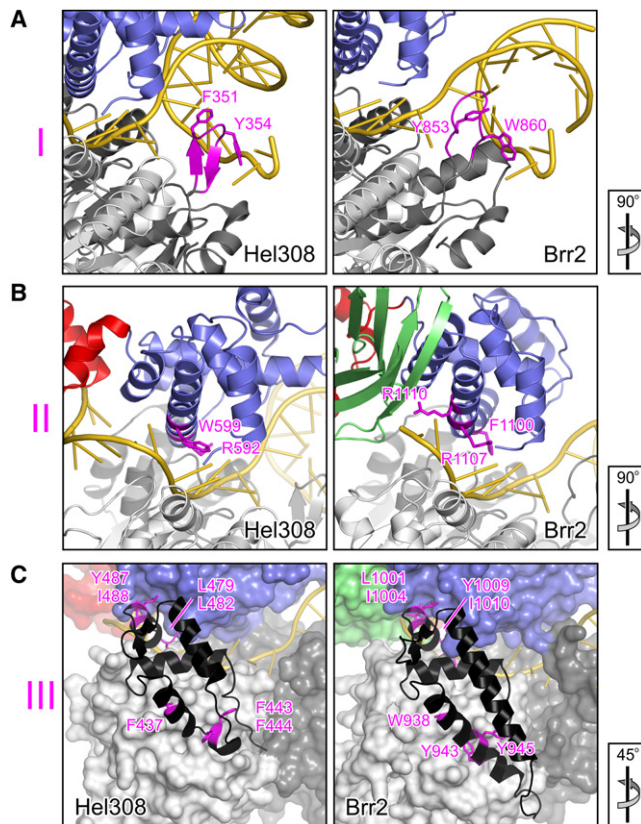


Figure 5. Model Features Investigated by Mutational Analysis

(A) Close-up view of the strand separation loop (I, magenta) of Hel308 (left) and in the model of the N-terminal cassette of Brr2. Aromatic residues in the loops that may interact with RNA bases are shown as sticks and labeled. Domains are colored as before. The views relative to Figure 2B, right panel, are indicated.

(B) Close-up view of the underside of helix $\alpha 5$ of the helical bundle domains of Hel308 (left) and of the N-terminal cassette of Brr2. Aromatic and positively charged residues extending toward the nucleic acid (gold) are shown as sticks and are labeled (II, magenta).

(C) Close-up view of residues of the WH domain that engage in contact with the first RecA-like domain and the helical bundle domain (III, magenta). Hel308 is shown on the left, and the model of the N-terminal cassette of Brr2 is shown on the right.

acid strands as in Hel308 (Figure 5A, right). We generated a mutant *brr2*, in which this loop (residues 851–862) was replaced by two alanines. As expected, if this loop acted as a strand separator, the deletion mutant did not support cell growth (Figure 6A). This interpretation is also in agreement with a recent analysis by Zhao and colleagues (Zhang et al., 2009).

The N-Terminal Sec63 Unit May Provide a Ratchet by Directly Contacting RNA

A fundamental question is how some helicases can processively unwind a nucleic acid duplex. One solution to this problem comes from regulatory elements that act as a ratchet, a principle that has first been observed in the NS3 helicase (Kim et al., 1998). Deletion of the helical bundle domain of Hel308 showed that it is essential for coupling of the ATPase activity to nucleic acid translocation, suggesting that, in Hel308, this domain also acts as

a ratchet (Buttner et al., 2007). It was proposed to employ positively charged (R592) and aromatic (W599) residues along its scaffolding helix (Figure 5B, left) to intermittently hold on to the DNA substrate during cycles of ATP hydrolysis and conformational rearrangements (Buttner et al., 2007).

In our model of the N-terminal cassette of Brr2, nucleic acid binding is complemented by the helical bundle domain of the Sec63^N unit, which forms the roof of the predicted single-stranded nucleic-acid-binding tunnel (Figure 5B, right). As in the case of Hel308, the scaffolding helix $\alpha 5$ of Sec63^N runs along the entire length of this tunnel, and aromatic (F1100) and positively charged side chains (R1107 and R1110) protrude from the underside of this helix and are predicted to directly interact with the RNA (Figure 5B, right). Although the positions of the aromatic and positively charged residues along helix $\alpha 5$ are shuffled compared to Hel308 (Figure S1), the underside of helix $\alpha 5$ of Sec63^N exhibits a similar chemical composition as in Hel308. These findings are consistent with the idea that the helical bundle domain of Sec63^N also acts as a ratcheting device that allows the N-terminal cassette of Brr2 to processively unwind RNA duplexes. A similar configuration is also seen in the N-terminal cassette of Slh1 and in Mer3/HFM1 (Figure S1). Notably, in the analogous positions of the Sec63^C unit in the C-terminal cassette of Brr2 (and of Slh1), aromatic or positively charged residues are not or are only partially conserved (Figure S1). A ratcheting function of Sec63^C would not be required if the C-terminal cassette had been converted into a pseudoenzyme that primarily served as an interaction platform. Translocon Sec63p exhibits an arginine and two histidines in the equivalent positions, whose functions are not clear.

In order to test the importance of the aromatic and positively charged residues on the underside of the Sec63^N unit, we mutated each of these residues individually to the corresponding residue of the C-terminal Sec63 unit (F1100D, R1107P, and R1110N). In addition, we generated the F1100D/R1107P double mutant. All mutations gave rise to cellular defects, albeit of different severity. The F1100D mutation alone had only minor effects on cell growth but was synthetically lethal in combination with R1107P (Figure 6B). The R1107P allele exhibited a cold-sensitive phenotype and showed reduced growth at 37°C (Figure 6B). An allele bearing the R1110N mutation did not support cell growth (Figure 6A).

We next tested whether the growth defects conferred by the mutant alleles originate from a direct effect on pre-mRNA splicing. To this end, we compared the *in vivo* splicing efficiency of yeast strains bearing mutant *brr2*^{F1100D} or *brr2*^{R1107P} to a WT control by assessing the accumulation of endogenous U3 snoRNA precursors (Vijayraghavan et al., 1989). In the presence of WT Brr2, no precursor forms were detected under our assay conditions at either 16°C, 25°C, or 37°C (Figure 6D, lanes 1–5), whereas the known cold-sensitive *brr2*^{E610G} mutant showed strong precursor accumulation at 16°C (lanes 6–8). Consistent with the mild growth defects (Figure 6B), the F1100D mutation led to only slight precursor accumulation at 16°C or 37°C (Figure 6D, lanes 9–13). The R1107P mutant, in contrast, gave rise to strong precursor accumulation at 16°C (Figure 6D, lanes 15 and 16) and to intermediate levels of precursor at 37°C (Figure 6D, lanes 17 and 18). In nice agreement with our findings,

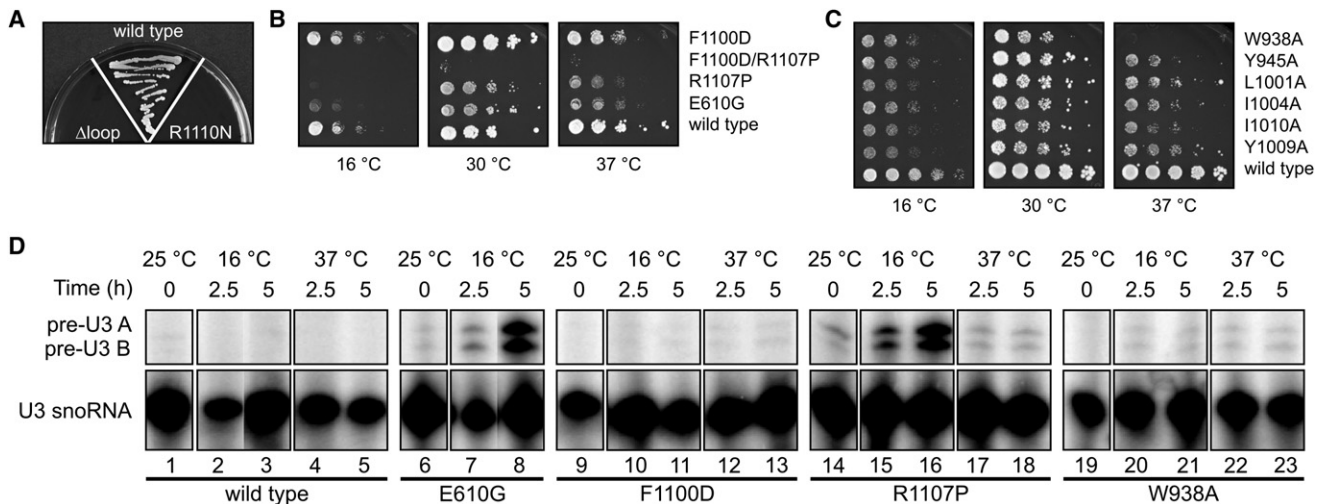


Figure 6. Mutational Analysis

(A–C) Growth of yeast cells that express WT Brr2 or *brr2* variants bearing the indicated mutations. *brr2*^{E610G} is expressed from plasmid pR151 and is known to confer a cold-sensitive phenotype (Ragunathan and Guthrie, 1998). Cells were plated in serial dilutions and grown for 2 days at the temperatures indicated. (D) In vivo splicing assay. Yeast cells expressing WT Brr2 or the indicated mutants were grown for 2.5 or 5 hr at 16 °C, 25 °C or 37 °C. After extraction of total RNA, two precursor forms of U3 snoRNA (pre-U3 A and pre-U3 B; top panels) and mature U3 snoRNA (bottom panels) were detected by primer extension. Accumulation of the U3 snoRNA precursors indicates a splicing defect conferred by the mutant *brr2*.

a different point mutation at position 1107, R1107A, has recently been shown to elicit a cold-sensitive phenotype in a screen for conditionally lethal mutants of the N-terminal Sec63 unit. Biochemical assays revealed that both the U4/U6 RNA unwinding and the intron release functions of Brr2 were compromised by this mutation (Small et al., 2006). In light of our model, these results support a role of the helical bundle domain of Sec63^N in nucleic acid binding. Furthermore, the results are in agreement with the idea that, similar to the Hel308 case, this domain may comprise a ratchet that could act to couple conformational changes to nucleic acid translocation.

The WH Domain May Functionally Integrate the RecA-like Domains and the Sec63 Unit

In order for the helical bundle domain of the Sec63^N unit to act as a ratchet, it has to be functionally connected to the RecA-like domains. In Hel308, a WH domain follows the second RecA-like domain and exhibits extensive interfaces both with the first RecA-like domain and with the helical bundle domain of the truncated Sec63 unit, forming one wall of the tunnel through which the 3' tail of one DNA strand is threaded. Its function has so far not been tested experimentally. Our models predict that, analogous to the organization of Hel308, in both cassettes of Brr2, a WH domain following the second RecA-like domain links up the first RecA-like domain and the helical bundle domain of the Sec63 unit through hydrophobic interfaces (Figure 5C). Residues lining these predicted interfaces are conserved in Brr2 (Figure S1) and lead to the same relative orientation of the WH domain with respect to the RecA-like and helical bundle domains as in Hel308. Therefore, we interrogated the putative function of the WH domain of the N-terminal Brr2 cassette as a connection device by replacing such hydrophobic interface residues of the WH domain with alanines and assessing the effect of the mutant

alleles on cell viability. All individual alanine mutants exhibited significant growth defects compared to WT Brr2 (Figure 6C). In particular, the W938A exchange gave rise to a temperature-sensitive phenotype (Figure 6C). We again confirmed, using the U3 reporter system, that the W938A mutant conferred a pre-mRNA splicing defect at 16 °C and 37 °C (Figure 6D, lanes 19–23). Together, these results are consistent with the idea that the WH domain acts as a positioning device for the Sec63 unit relative to the catalytic RecA-like domains. The contact residues on the WH domain are expected to contribute additively to the domain interfaces so that removal of an individual side chain would most likely be accompanied by a mild defect as observed.

Mutations in the Presumed Ratchet Helix or the WH Connector Affect RNA Unwinding

In order to directly test whether the presumed ratchet helix of the Sec63^N unit and the WH domain are important for RNA duplex unwinding by Brr2, we tested the unwinding activity of highly purified (Figure S5) WT and mutant Brr2 in vitro on full-length U4/U6 RNA.

In contrast to a recent report (Zhang et al., 2009), we found that WT Brr2 alone efficiently unwound U4/U6 RNA (Figure 7A), using gel-purified RNA substrate that essentially lacked single-stranded RNA. As reported recently (Maeder et al., 2009), the unwinding was further stimulated by a C-terminal portion of Prp8 (Prp8^{1796–2092}) (Figure 7A). In order to investigate the Prp8 effect in greater detail, we quantified the time courses of unwinding in the absence and presence of Prp8^{1796–2092}, using equimolar amounts of enzyme and substrate (Figure 7A) and excess concentration of enzyme to substrate (Figure S6). Prp8^{1796–2092} enabled the reaction to go to near completion within 1 hr when the substrate concentration was similar to that of Brr2. In contrast, at limiting substrate concentration, neither the initial

rate nor the reaction amplitude was significantly altered by Prp8^{1796–2092}. A likely explanation for the effect of Prp8 on the Brr2-catalyzed unwinding is that it increases the association rate of Brr2 with the substrate, in agreement with recent RNA binding studies (Zhang et al., 2009). Under our multiple turnover conditions, Brr2 can reassociate more rapidly with the substrate after dissociation from the product in the presence of Prp8^{1796–2092}, resulting in increased product formation. Consistent with this interpretation, the effect of Prp8 was negligible when Brr2 exceeded the substrate (Figure S6). The same effect has previously been reported for the processive hepatitis C virus NS3 helicase stimulated by the NS5B polymerase (Jennings et al., 2008).

The unwinding of the truncated U4^{1–64}/U6^{55–81} duplex under limiting substrate conditions (Figure 7B) showed a 7-fold reduced initial rate and 2-fold lower amplitude, which may indicate weak binding of Brr2 and therefore slower assembly of functional enzyme-RNA complexes. The increased product formation observed with the full-length U4/U6 RNA suggests that functional complexes are formed more rapidly when Brr2 can load on single-stranded overhangs of the substrate. Brr2 most likely binds breathing termini of the U4^{1–64}/U6^{55–81} duplex, given that it failed to unwind U4^{1–64}/U6^{55–81} RNA in the presence of Snu13 (Figure 7C). In contrast, unwinding of full-length U4/U6 RNA was attenuated but still significant in the presence of Snu13 (Figure 7C). The detailed effects of U4/U6 proteins on the activity of Brr2 will be subject to future studies.

Mutant brr2 proteins tested here were equally well expressed and purified as WT Brr2 (Figure S5), suggesting that the mutants did not suffer from global misfolding. U4/U6 RNA unwinding was abrogated in brr2^{R1110N} and could not be regained by addition of Prp8^{1796–2092} (Figure 7D), explaining why brr2^{R1110N} fails to support cell viability. The result also confirms the importance of the presumed ratchet helix of Sec63^N in RNA unwinding by Brr2. The brr2^{W938Q} variant, in which a presumed contact residue (W938) to the first RecA-like domain was exchanged, showed strongly reduced U4/U6 RNA unwinding, but the activity could be stimulated by Prp8^{1796–2092} (Figure 7D). The partial rescue by Prp8^{1796–2092} further confirms that brr2^{W938Q} can adopt a native fold. The behavior of brr2^{W938Q} can be explained by our suggestion that the WH domain may act as a positioning device for the active site modules. Mutating an interface residue may have less-severe consequences than mutation of a presumed RNA-contacting residue (e.g., R1110N) because additional contact points in the interface would dampen the effect of a point mutation.

Conclusions

Apart from the conserved RecA-like catalytic modules, nucleic acid unwindases frequently harbor accessory domains that influence catalytic activities or mediate interaction with other factors. The spliceosomal Brr2 helicase encompasses helicase-associated Sec63 units of unknown function. Work presented here suggests that the dual RecA-like domains and the helical bundle domain of the Sec63 unit form a functional entity, whose integrity is maintained by a WH connector. It is possible that, analogous to the situation in Hel308, this architecture serves to integrate a ratcheting device on the Sec63 unit (the helical bundle domain) with the catalytic RecA-like domains.

Alternatively, the Sec63 unit may support RNA binding without ratcheting. It is tempting to suggest that this functional combination may allow Brr2 to processively plow through extended RNA duplexes such as the U4/U6 duplex during spliceosome catalytic activation. Dissociation of proteins from the U4/U6 RNA during catalytic activation could result indirectly from Brr2 taking apart the underlying RNA duplex.

Presently, there is no direct evidence for processivity in Brr2. However, our studies show that Brr2 preferentially binds and unwinds substrates with single-stranded overhangs compared to substrates lacking overhangs. Brr2 bound U4/U6 RNA even in the absence of ATP (Figures 4 and S7) or in the presence of a nonhydrolyzable ATP analog, yet this binding was not accompanied by RNA unwinding. Furthermore, Brr2 efficiently unwound the extensively base-paired U4/U6 duplex from yeast but was much less active on a truncated duplex. Furthermore, we present evidence that regulation of Brr2 by Prp8^{1796–2092} parallels the regulation of the processive NS3 helicase by the NS5B polymerase (Jennings et al., 2008). Thus, Brr2 exhibits characteristics expected from a processive, translocating helicase. Our findings are more difficult to reconcile with the idea that Brr2 should follow a punctuated, nonprocessive mechanism.

In SF2 helicases, nucleic acid substrates preferentially bind with a 3'-to-5' directionality across the first and second RecA-like domains, which could explain the 3'-to-5' unwinding directionality commonly observed with these enzymes (Hopfner and Michaelis, 2007). In particular, a 3'-to-5' translocation has been experimentally confirmed for Hel308 (Guy and Bolt, 2005), Mer3/HFM1 (Nakagawa and Kolodner, 2002), and Mtr4 (Bernstein et al., 2008), which are all members of the Ski2-like subfamily to which also Brr2 belongs (Bleichert and Baserga, 2007). Thus, it is expected that Brr2 also acts by translocating in the 3'-to-5' direction on its nucleic acid substrates.

Considering that U6 RNA is a common factor in spliceosome catalytic activation (unwinding of the U4/U6 duplex) and disassembly (unwinding of U2/U6 and intron/U6 duplexes), i.e., in the two processes during which Brr2 is required, Brr2 may “walk” on the U6 RNA (Small et al., 2006). Together, these considerations predict that Brr2 first unwinds stem II of the U4/U6 RNA interaction region, followed by unwinding of stem I. However, in the minor spliceosome, Frilander and Steitz have observed an intermediate on the path to catalytic activation that still contained an intact U4atac/U6atac stem II but in which the U4atac/U6atac stem I was already replaced by a U12/U6atac helix Ia interaction (Frilander and Steitz, 2001). In the context of our results, this finding could be explained (1) if Brr2 only was required for unwinding of stem II, (2) if it translocated on U4atac (and by analogy on U4) in a 3'-to-5' direction, (3) if it walked in the opposite direction on U6atac (or U6), or (4) if the intermediate detected represented an alternative, noncanonical pathway for catalytic activation. Recent mapping of constituents on the electron microscopic structure of the yeast U4/U6-U5 tri-snRNP (Hacker et al., 2008) are consistent with a model in which U4/U6 RNA stem II coaxially stacks on a U4 5' stem loop (Lescoute and Westhof, 2006) forming a separate domain from stem I. This organization would be consistent with Brr2 and another helicase dissociating stem II and stem I,

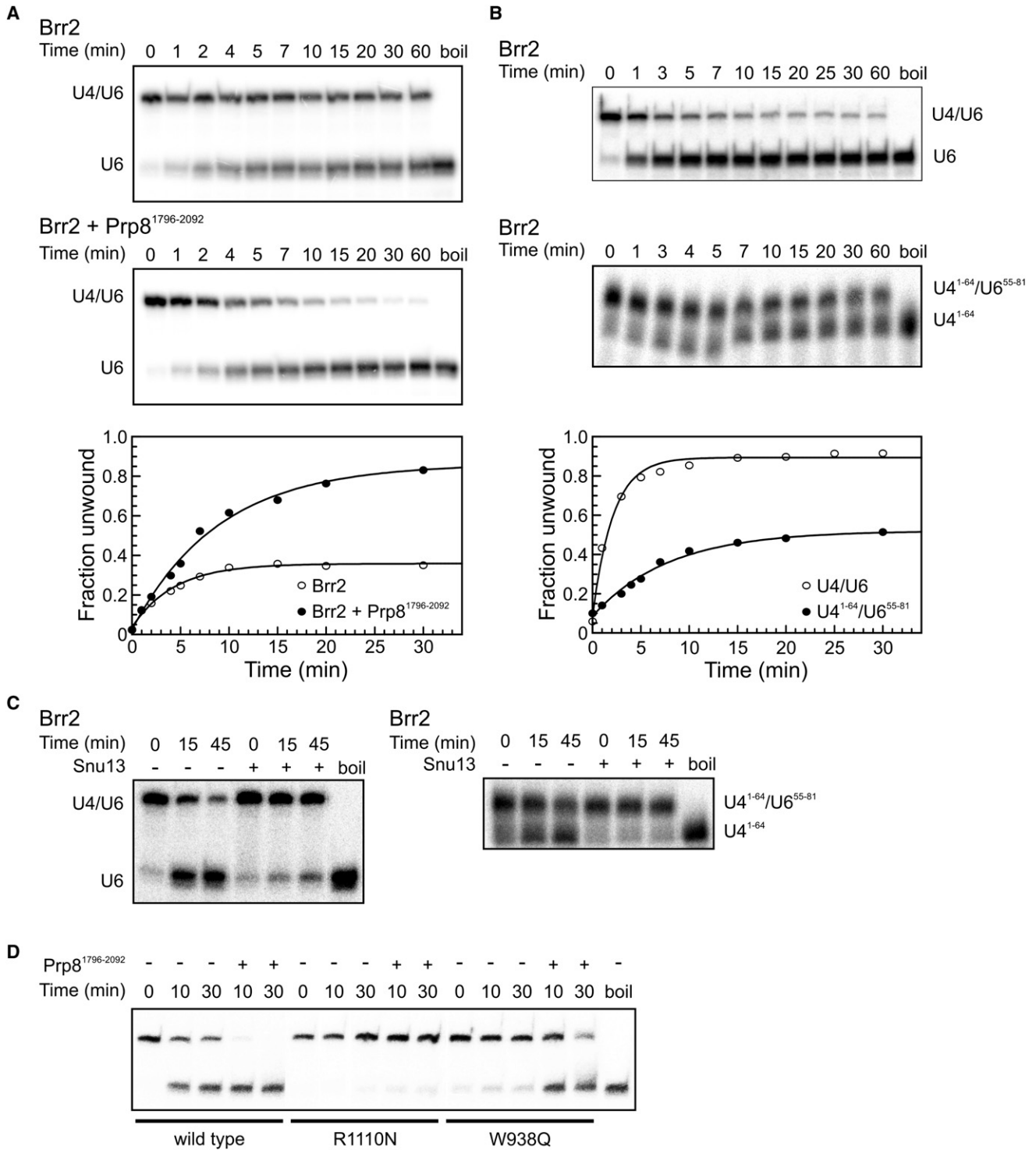


Figure 7. Duplex Unwinding by Wild-Type and Mutant Brr2

(A) (Top) Time course of the unwinding of U4/U6 RNA (2.5 nM; U6 labeled) by an equimolar amount of Brr2 (2.5 nM) at 40°C. After preincubation of substrate with Brr2 for 3 min at 40°C, the reaction was started with 2 mM ATP/MgCl₂. (Middle) Effect of Prp8¹⁷⁹⁶⁻²⁰⁹² on the unwinding activity of Brr2. Except for the presence of Prp8¹⁷⁹⁶⁻²⁰⁹² (250 nM), the experimental conditions were identical to those in the top panel. (Bottom) Quantification of the unwinding activity in the absence (open circles) and presence (closed circles) of Prp8¹⁷⁹⁶⁻²⁰⁹². Data were fit to the equation: fraction unwound = A[1 - exp(-k_u t)] + k₂ t; A, amplitude of the reaction; k_u, apparent first-order rate constant for unwinding; k₂, steady-state rate; t, time. The amplitude of the reaction is increased in the presence of Prp8¹⁷⁹⁶⁻²⁰⁹² (A(Brr2) = 0.34 ± 0.02; A(Brr2 + Prp8¹⁷⁹⁶⁻²⁰⁹²) = 0.81 ± 0.05), whereas the rate constant is affected little (k_u(Brr2) = 0.29 ± 0.04 min⁻¹, k_u(Brr2 + Prp8¹⁷⁹⁶⁻²⁰⁹²) = 0.13 ± 0.01 min⁻¹).

respectively. Definitive answers to these questions will require further experimental tests.

Being a resident factor of the spliceosome, Brr2 requires special regulatory mechanisms to precisely time its activities. A C-terminal fragment of Prp8 has been found to couple ATP hydrolysis by Brr2 to RNA unwinding (Maeder et al., 2009). Interestingly, the helical bundle domain of the truncated Sec63 unit of Hel308 is also required for the coupling of ATPase activity to nucleic acid translocation (Buttner et al., 2007). Thus, Prp8 may exert its effect via the N-terminal Sec63 unit of Brr2. Yeast two-hybrid data (Liu et al., 2006; van Nues and Beggs, 2001) and pull-down experiments (Zhang et al., 2009) suggest that Prp8^{1796–2092} interacts with the C-terminal cassette of Brr2. Prp8^{1796–2092} may also contact the N-terminal cassette, or binding of Prp8^{1796–2092} to the C-terminal cassette may be communicated to the N-terminal cassette by a direct contact between the two cassettes of Brr2. Our observation that Prp8^{1796–2092} can partially rescue the U4/U6 RNA unwinding activity of the *brr2*^{W938Q} mutant suggests that Prp8^{1796–2092} binding directly or indirectly leads to stabilization or structural rearrangements in the N-terminal cassette. Alternatively or in addition, Prp8 could influence RNA binding by Brr2 or interfere with crucial protein-protein interactions at the C-terminal Sec63 unit. Additional functional analyses and an experimental structure of the dual cassette arrangement are required to clarify these points.

EXPERIMENTAL PROCEDURES

Details of the expression, purification, and crystal structure analysis, as well as the bioinformatics analyses and RNA binding and unwinding assays, are given in the Supplemental Experimental Procedures.

Site-Directed Mutagenesis and Cell Viability Assay

The desired mutations were introduced into the *BRR2* gene of plasmid pR150 (Raghuathan and Guthrie, 1998) by the QuikChange Site-Directed Mutagenesis strategy (Stratagene) and verified by sequencing. WT Brr2 expressed from plasmid pR150 and *brr2*^{E610G} expressed from plasmid pR151 (known to elicit a cold-sensitive phenotype; Raghuathan and Guthrie, 1998) served as controls. WT and mutant plasmids were transformed into the yeast strain PRY118 (kindly provided by Christine Guthrie, University of California, San Francisco, USA), which expresses WT Brr2 on a counter-selectable *ura3*-marked plasmid (Brown and Beggs, 1992). Before plasmid shuffling, cells were selected at 25°C in medium lacking histidine. Transformants were streaked once on medium lacking histidine, grown at 25°C, and then restreaked three times on 5-FOA plates to select for cells lacking the *ura3* plasmid. Cells that survived on 5-FOA were streaked on rich medium, and their growth phenotypes were analyzed by incubating about 5×10^4 cells and serial 8-fold dilutions at 37°C, 30°C, 25°C, and 16°C for 1 or 2 days. All cells that survived on 5-FOA plates failed to grow on plates lacking Ura.

In Vivo Splicing Assay

Fresh prewarmed YP medium containing 2% glucose was inoculated to an initial OD₆₀₀ of 0.05 with yeast strain PRY118, which bore either plasmid pR150 or mutant variants and survived on 5-FOA plates. Cells were grown at the selected temperatures, and aliquots were taken at specified time points. Total RNA was extracted from the aliquots, and 5 μg from each sample together with 15×10^4 cpm of radiolabeled oligonucleotide were used for primer extension as described (Vijayraghavan et al., 1989) in order to visualize accumulation of two forms of U3 snoRNA precursor at nonpermissive temperatures. The primer extension runs were analyzed on 8% polyacrylamide/8 M urea gels and visualized via a phosphorimager.

ACCESSION NUMBERS

The diffraction data and structure coordinates have been deposited with the Protein Data Bank (<http://www.pdb.org/>) under PDB IDs 3IM1 (form 1) and 3IM2 (form 2).

SUPPLEMENTAL DATA

Supplemental Data include Supplemental Experimental Procedures and seven figures and can be found with this article online at [http://www.cell.com/molecular-cell/supplemental/S1097-2765\(09\)00552-8](http://www.cell.com/molecular-cell/supplemental/S1097-2765(09)00552-8).

ACKNOWLEDGMENTS

Yeast strain PRY118 and the plasmids pR150 and pR151 were kind gifts from Christine Guthrie (University of California, San Francisco, USA). We thank Kristian Rother (IIMCB) for help with RNA modeling; Karine dos Santos and Homa Ghalei (MPI Biophysical Chemistry) for preparation of Prp8^{1796–2092} and of Snu13, respectively; Elke Penka (MPI Biophysical Chemistry) for technical assistance; Liudmila Filonava and Marina Rodnina (MPI Biophysical Chemistry) for help with analysis of unwinding kinetics; Klaus Hartmuth (MPI Biophysical Chemistry) for helpful discussions; and the team of beamline BW6 (DESY, Hamburg, Germany) for support during diffraction data collection. This work was supported by the EURASNET Network of Excellence in the 6th Framework Program of the European Commission (J.O., J.M.B., and R.L.), the Volkswagen Stiftung (R.L. and M.C.W.), and the Ernst-Jung-Stiftung (R.L.).

Received: April 14, 2009

Revised: July 17, 2009

Accepted: August 12, 2009

Published: August 27, 2009

REFERENCES

- Bernstein, J., Patterson, D.N., Wilson, G.M., and Toth, E.A. (2008). Characterization of the essential activities of Saccharomyces cerevisiae Mtr4p, a 3'->5' helicase partner of the nuclear exosome. *J. Biol. Chem.* 283, 4930–4942.
- Bessonov, S., Anokhina, M., Will, C.L., Urlaub, H., and Lührmann, R. (2008). Isolation of an active step I spliceosome and composition of its RNP core. *Nature* 452, 846–850.

(B) (Top) Time course of the unwinding of full-length U4/U6 RNA (0.25 nM; U6 labeled) by 100-fold molar excess of Brr2 (25 nM). (Middle) Time course of the unwinding of U4^{1–64}/U6^{55–81} RNA (0.25 nM; U4^{1–64} labeled) by 100-fold molar excess of Brr2 (25 nM). The enzyme-substrate mixtures were preincubated for 3 min at room temperature and for 2 min at 40°C prior to initiation of the reactions by addition of 2 mM ATP/MgCl₂. (Bottom) Quantification of the unwinding activity of Brr2 on U4/U6 RNA (open circles) and on U4^{1–64}/U6^{55–81} RNA (closed circles). Data were fit to the equation: fraction unwound = $A\{1 - \exp(-k_u t)\}$; A , amplitude of the reaction; k_u , apparent first-order rate constant for unwinding; t , time. The linear portions of each plot (0–2 min) were used to calculate observed initial rates (R) by linear regression. The initial rate and reaction amplitude are strongly reduced when the substrate lacks single-stranded overhangs. ($A(U4/U6) = 0.90 \pm 0.01$; $A(U4^{1-64}/U6^{55-81}) = 0.52 \pm 0.01$; $k_u(U4/U6) = 0.47 \pm 0.05 \text{ min}^{-1}$; $k_u(U4^{1-64}/U6^{55-81}) = 0.13 \pm 0.01 \text{ min}^{-1}$; $R(U4/U6) = 72.35 \pm 6.5 \text{ fM} \cdot \text{min}^{-1}$; $R(U4^{1-64}/U6^{55-81}) = 10.17 \pm 1.22 \text{ fM} \cdot \text{min}^{-1}$). (C) Unwinding of WT U4/U6 RNA (0.25 nM; U6 labeled; left) and of U4^{1–64}/U6^{55–81} RNA (0.25 nM; U4^{1–64} labeled; right) by a 100-fold molar excess of Brr2 (25 nM) in the presence of 1 μM Snu13. Substrates were preincubated with Snu13 for 20 min at 4°C and after addition of Brr2 for an additional 3 min at 30°C. Unwinding was started by addition of ATP/MgCl₂ (2 mM) and monitored at 30°C.

(D) Unwinding of U4/U6 RNA (0.2 nM; U6 labeled) by WT and mutant Brr2 (2 mM ATP; 40°C) in the absence or presence of Prp8^{1796–2092} (250 nM; indicated).

- Bleichert, F., and Baserga, S.J. (2007). The long unwinding road of RNA helicases. *Mol. Cell* 27, 339–352.
- Brow, D.A. (2002). Allosteric cascade of spliceosome activation. *Annu. Rev. Genet.* 36, 333–360.
- Brow, D.A., and Guthrie, C. (1988). Spliceosomal RNA U6 is remarkably conserved from yeast to mammals. *Nature* 334, 213–218.
- Brown, J.D., and Beggs, J.D. (1992). Roles of PRP8 protein in the assembly of splicing complexes. *EMBO J.* 11, 3721–3729.
- Buttner, K., Nehring, S., and Hopfner, K.P. (2007). Structural basis for DNA duplex separation by a superfamily-2 helicase. *Nat. Struct. Mol. Biol.* 14, 647–652.
- Davis, I.W., Murray, L.W., Richardson, J.S., and Richardson, D.C. (2004). MOLPROBITY: structure validation and all-atom contact analysis for nucleic acids and their complexes. *Nucleic Acids Res.* 32, W615–W619.
- Frilander, M.J., and Steitz, J.A. (2001). Dynamic exchanges of RNA interactions leading to catalytic core formation in the U12-dependent spliceosome. *Mol. Cell* 7, 217–226.
- Guy, C.P., and Bolt, E.L. (2005). Archaeal Hel308 helicase targets replication forks in vivo and in vitro and unwinds lagging strands. *Nucleic Acids Res.* 33, 3678–3690.
- Hacker, I., Sander, B., Golas, M.M., Wolf, E., Karagoz, E., Kastner, B., Stark, H., Fabrizio, P., and Lührmann, R. (2008). Localization of Prp8, Brr2, Snu114 and U4/U6 proteins in the yeast tri-snRNP by electron microscopy. *Nat. Struct. Mol. Biol.* 15, 1206–1212.
- Hopfner, K.P., and Michaelis, J. (2007). Mechanisms of nucleic acid translocases: lessons from structural biology and single-molecule biophysics. *Curr. Opin. Struct. Biol.* 17, 87–95.
- Jennings, T.A., Chen, Y., Sikora, D., Harrison, M.K., Sikora, B., Huang, L., Jankowsky, E., Fairman, M.E., Cameron, C.E., and Raney, K.D. (2008). RNA unwinding activity of the hepatitis C virus NS3 helicase is modulated by the NS5B polymerase. *Biochemistry* 47, 1126–1135.
- Kim, D.H., and Rossi, J.J. (1999). The first ATPase domain of the yeast 246-kDa protein is required for in vivo unwinding of the U4/U6 duplex. *RNA* 5, 959–971.
- Kim, J.L., Morgenstern, K.A., Griffith, J.P., Dwyer, M.D., Thomson, J.A., Murcko, M.A., Lin, C., and Caron, P.R. (1998). Hepatitis C virus NS3 RNA helicase domain with a bound oligonucleotide: the crystal structure provides insights into the mode of unwinding. *Structure* 6, 89–100.
- Kosinski, J., Gajda, M.J., Cymerman, I.A., Kurowski, M.A., Pawlowski, M., Boniecki, M., Obarska, A., Papaj, G., Sroczynska-Obuchowicz, P., Tkaczuk, K.L., et al. (2005). FFrankenstein becomes a cyborg: the automatic recombination and realignment of fold recognition models in CASP6. *Proteins* 61 (Suppl 7), 106–113.
- Kurowski, M.A., and Bujnicki, J.M. (2003). GeneSilico protein structure prediction meta-server. *Nucleic Acids Res.* 31, 3305–3307.
- Laggerbauer, B., Achsel, T., and Lührmann, R. (1998). The human U5-200kD DEXH-box protein unwinds U4/U6 RNA duplexes in vitro. *Proc. Natl. Acad. Sci. USA* 95, 4188–4192.
- Lam, A.M., Keeney, D., and Frick, D.N. (2003). Two novel conserved motifs in the hepatitis C virus NS3 protein critical for helicase action. *J. Biol. Chem.* 278, 44514–44524.
- Lauber, J., Fabrizio, P., Teigelkamp, S., Lane, W.S., Hartmann, E., and Lührmann, R. (1996). The HeLa 200 kDa U5 snRNP-specific protein and its homologue in *Saccharomyces cerevisiae* are members of the DEXH-box protein family of putative RNA helicases. *EMBO J.* 15, 4001–4015.
- Lescoute, A., and Westhof, E. (2006). Topology of three-way junctions in folded RNAs. *RNA* 12, 83–93.
- Liu, S., Rauhut, R., Vornlocher, H.P., and Lührmann, R. (2006). The network of protein-protein interactions within the human U4/U6.U5 tri-snRNP. *RNA* 12, 1418–1430.
- Liu, S., Li, P., Dybkov, O., Nottrott, S., Hartmuth, K., Lührmann, R., Carlomagno, T., and Wahl, M.C. (2007). Binding of the human Prp31 Nop domain to a composite RNA-protein platform in U4 snRNP. *Science* 316, 115–120.
- Maeder, C., Kutach, A.K., and Guthrie, C. (2009). ATP-dependent unwinding of U4/U6 snRNAs by the Brr2 helicase requires the C terminus of Prp8. *Nat. Struct. Mol. Biol.* 16, 42–48.
- Martegani, E., Vanoni, M., Mauri, I., Rudoni, S., Saliola, M., and Alberghina, L. (1997). Identification of gene encoding a putative RNA-helicase, homologous to SKI2, in chromosome VII of *Saccharomyces cerevisiae*. *Yeast* 13, 391–397.
- Nakagawa, T., and Kolodner, R.D. (2002). The MER3 DNA helicase catalyzes the unwinding of Holliday junctions. *J. Biol. Chem.* 277, 28019–28024.
- Noble, S.M., and Guthrie, C. (1996). Identification of novel genes required for yeast pre-mRNA splicing by means of cold-sensitive mutations. *Genetics* 143, 67–80.
- Pawlowski, M., Gajda, M.J., Matlak, R., and Bujnicki, J.M. (2008). MetaMQAP: a meta-server for the quality assessment of protein models. *BMC Bioinformatics* 9, 403.
- Ponting, C.P. (2000). Proteins of the endoplasmic-reticulum-associated degradation pathway: domain detection and function prediction. *Biochem. J.* 351, 527–535.
- Raghuathan, P.L., and Guthrie, C. (1998). RNA unwinding in U4/U6 snRNPs requires ATP hydrolysis and the DEIH-box splicing factor Brr2. *Curr. Biol.* 8, 847–855.
- Small, E.C., Leggett, S.R., Winans, A.A., and Staley, J.P. (2006). The EF-G-like GTPase Snu114p regulates spliceosome dynamics mediated by Brr2p, a DEXH/H box ATPase. *Mol. Cell* 23, 389–399.
- Staley, J.P., and Guthrie, C. (1998). Mechanical devices of the spliceosome: motors, clocks, springs, and things. *Cell* 92, 315–326.
- Tanner, N.K., and Linder, P. (2001). DEXH/H box RNA helicases: from generic motors to specific dissociation functions. *Mol. Cell* 8, 251–262.
- van Nues, R.W., and Beggs, J.D. (2001). Functional contacts with a range of splicing proteins suggest a central role for Brr2p in the dynamic control of the order of events in spliceosomes of *Saccharomyces cerevisiae*. *Genetics* 157, 1451–1467.
- Vidovic, I., Nottrott, S., Hartmuth, K., Lührmann, R., and Ficner, R. (2000). Crystal structure of the spliceosomal 15.5kD protein bound to a U4 snRNA fragment. *Mol. Cell* 6, 1331–1342.
- Vijayraghavan, U., Company, M., and Abelson, J. (1989). Isolation and characterization of pre-mRNA splicing mutants of *Saccharomyces cerevisiae*. *Genes Dev.* 3, 1206–1216.
- Wahl, M.C., Will, C.L., and Lührmann, R. (2009). The spliceosome: design principles of a dynamic RNP machine. *Cell* 136, 701–718.
- Yang, Q., Del Campo, M., Lambowitz, A.M., and Jankowsky, E. (2007). DEAD-box proteins unwind duplexes by local strand separation. *Mol. Cell* 28, 253–263.
- Zhang, L., Xu, T., Maeder, C., Bud, L.O., Shanks, J., Nix, J., Guthrie, C., Pleiss, J.A., and Zhao, R. (2009). Structural evidence for consecutive Hel308-like modules in the spliceosomal ATPase Brr2. *Nat. Struct. Mol. Biol.* 16, 731–739.